

Nearby Supernova Rates from the Lick Observatory Supernova Search. IV. A Recovery Method for the Delay Time Distribution

Dan Maoz^{1*}, Filippo Mannucci², Weidong Li³, Alexei V. Filippenko³,
Massimo Della Valle⁴, Nino Panagia^{5,6,7}

¹*School of Physics and Astronomy, Tel-Aviv University, Tel-Aviv 69978, Israel*

²*INAF-Istituto di Radioastronomia, Largo Enrico Fermi 5, Firenze 50125, Italy*

³*Department of Astronomy, University of California, Berkeley, CA 94720-3411, USA*

⁴*INAF-Osservatorio Astronomico di Capodimonte, Salita Moiariello 16, Napoli 80131, Italy*

⁵*Space Telescope Science Institute, 3700 San Martin Drive, Baltimore, MD 21218, USA*

⁶*INAF - Osservatorio Astrofisico di Catania, Via Santa Sofia 78, I-95123 Catania, Italy*

⁷*Supernova Ltd., OYV #131, Northsound Road, Virgin Gorda, British Virgin Islands*

13 March 2019

ABSTRACT

Recovery of the supernova (SN) delay-time distribution (DTD) – the SN rate versus time that would follow a brief burst of star formation – can shed light on SN progenitors and physics, as well as on the timescales of chemical enrichment. Previous attempts to reconstruct the DTD have been based either on comparison of mean SN rates versus redshift to cosmic star-formation history (SFH), or on the comparison of SN rates among galaxies with different mean ages. Here, we present an approach to recover the SN DTD that avoids the averaging and loss of information of other schemes. We compare the SFHs of *individual* galaxies to the numbers of SNe discovered by a survey in each galaxy (generally zero, sometimes one SN, rarely a few). We apply the method to a subsample of 3505 galaxies, hosting 82 type-Ia SNe (SNe Ia) and 119 core-collapse supernovae (CC SNe), from the Lick Observatory SN Search (LOSS), that have SFHs reconstructed from Sloan Digital Sky Survey (SDSS) spectra. We find a $> 2\sigma$ SN Ia DTD signal in our shortest-delay, “prompt” bin at < 420 Myr. We identify and study a systematic error, due to the limited aperture of the SDSS spectroscopic fibres, that causes some of the prompt signal to leak to the later bins of the DTD. Nevertheless we demonstrate that a prompt SN Ia contribution is required by the data at the $> 99\%$ confidence level. We further find a 4σ indication of SNe Ia that are “delayed” by > 2.4 Gyr. Thus, the data support the existence of both prompt and delayed SNe Ia. We measure the time integral over the SN DTD. For CC SNe we find a total yield of 0.010 ± 0.002 SNe per M_{\odot} formed, in excellent agreement with expectations, if all stars more massive than $8 M_{\odot}$ lead to visible SN explosions. This argues against scenarios in which the minimum mass for core-collapse SNe is $\gtrsim 10 M_{\odot}$, or in which a significant fraction of massive stars collapse without an accompanying explosion. For SNe Ia, the time-integrated yield is 0.0023 ± 0.0006 SNe per M_{\odot} formed, most of them with delays < 2.4 Gyr. Finally, we show the robust performance of the method on simulated samples, and demonstrate that its application to already-existing SN samples, such as the full LOSS sample, but with complete and unbiased SFH estimates for the survey galaxies, could provide an accurate and detailed measurement of the SN Ia DTD.

Key words: supernovae: general — methods: data analysis

1 INTRODUCTION

Supernovae (SNe) figure prominently in many fields, whether in their roles as calibratable candles for cosmol-

* E-mail: maoz@astro.tau.ac.il

ogy, as the major sources of intermediate-mass and heavy elements, as heaters of the interstellar medium, as accelerators of cosmic rays, and more. Physically, they are separated mainly into core-collapse SNe (CC SNe), which occur when the iron core of a massive star collapses to form a neutron star or a black hole, and type-Ia SNe (SNe Ia), which explode when a degenerate carbon-oxygen stellar core, probably a white dwarf (WD), approaches (or, rarely, exceeds) the Chandrasekhar mass, igniting the carbon and triggering a thermonuclear runaway. The two paths most often hypothesised for this mass growth in SNe Ia are the single-degenerate (SD) scenario, whereby a WD in a semidetached binary accretes matter from a main-sequence or evolved normal companion star (Whelan & Iben 1974), and the double-degenerate (DD) scenario, in which two WDs merge (Iben & Tutukov 1984; Webbink 1984). Additional, less conventional, paths have also been considered (e.g., Tout 2005; Maoz & Mannucci 2008; Raskin et al. 2009a; Rosswog et al. 2009).

For CC SNe, while many questions remain regarding the progenitors and the physics of particular subtypes, massive progenitor stars have by now been identified in pre-explosion images in a growing number of cases (see Smartt et al. 2009, for a recent summary). This contrasts with the situation for SNe Ia, where only one or two very ambiguous progenitor identifications exist (Voss & Nelemans 2008; Roelofs et al. 2008; González Hernández et al. 2009; Kerzendorf et al. 2009). We thus do not quite know what is exploding in a SN Ia, an unsatisfactory situation given the ubiquity and importance of these events.

Driven by these problems, a major objective of SN studies has been the recovery of the SN delay-time distribution (DTD). The DTD is the SN rate as a function of time that would be observed following a δ -function burst of star formation. (In other contexts, the DTD would be called the delay function, the transfer function, or the Green’s function.) Knowledge of the DTD would be useful for understanding the route along which cosmic metal enrichment and energy input by SNe proceed, but no less important, for obtaining clues about the SN progenitor systems. Different progenitor stars, binary systems, and binary-evolution scenarios predict different DTDs.

The lifetime of a star with the minimum initial mass that is thought to lead to a CC SN explosion, $\gtrsim 8 M_{\odot}$, sets a time division between CC SNe and SNe Ia in the DTD, at ~ 40 Myr. The precise mass border between core collapse and WD formation also depends on metallicity. Furthermore, initially lower-mass stars in tight binaries can become “rejuvenated” by mass transfer and explode as CC SNe somewhat later than this.

For SNe Ia, the situation is much less clear. In both of the currently popular progenitor scenarios, SD and DD, calculations of the DTD depend on a series of assumptions regarding initial conditions (initial mass function, binarity fraction, mass-ratio distribution, separation distribution), and complex physics (mass loss, mass transfer, common-envelope evolution, accretion) that is sometimes computationally intractable except in the most rudimentary, parametrized forms (e.g., Hurley et al. 2002; Han & Podsiadlowski 2004; Nelemans et al. 2005; Ruiter et al. 2009; Bogomazov & Tutukov 2009; Meng & Yang 2010; Mennekens et al. 2010). In principle, observational estimates of the DTD could rule out particular theoretical models. Given the the-

oretical uncertainties, it is probably more realistic that the observations simply provide a ground truth that successful models will need to reproduce.

Previous attempts to recover the DTD have used SN rates measured in surveys of galaxies at different redshifts (i.e., different cosmic times), compared to cosmic star-formation histories (SFHs). This has been attempted for field surveys (Gal-Yam & Maoz 2004; Strolger et al. 2004; Poznanski et al. 2007; Dahlen et al. 2008) and galaxy-cluster surveys (Maoz & Gal-Yam 2004; Maoz et al. 2010). An alternative approach has been to look at the SN rates per unit stellar mass in galaxies of particular types (star forming, quiescent, etc.), and to attempt to assign to each type a “formation age,” or some generic, simple, SFH (e.g., Mannucci et al. 2005, 2006; Sullivan et al. 2006; Totani et al. 2008; Pritchett et al. 2008; Raskin et al. 2009b).

Results have been controversial and often contradictory. For example, Dahlen et al. (2004, 2008) have argued for a SN Ia DTD that is peaked at a delay of ~ 3 Gyr, with few SNe Ia at delays that are much shorter or longer. In contrast, Mannucci et al. (2005, 2006), Scannapieco & Bildsten (2005), and Sullivan et al. (2006) have found evidence for the existence of comparable numbers of both of “prompt” and “delayed” SNe Ia: the former explode within ~ 500 Myr (or perhaps even within 100 Myr) of star formation¹, while the latter may have delays as long as 10 Gyr. The SN Ia rate has been described as the sum of two components, one proportional to stellar mass and the other proportional to the CC SN rate (Mannucci et al. 2005). In the similar “ $A + B$ ” parameterisation introduced by Scannapieco & Bildsten (2005), the prompt-component rate is proportional to the star-formation rate (SFR). The two SN Ia components need not represent two distinct physical populations. Instead, they could constitute the SNe included in two coarsely sampled time bins of what is in reality a continuous DTD. For example, Pritchett et al. (2008) have argued that a $t^{-0.5 \pm 0.2}$ power-law DTD provides an improved fit, compared to the $A + B$ model, to the dependence of SN rates on galaxy SFR, as measured in the Supernova Legacy Survey. We also note that a truly bimodal DTD, if it exists, could arise either from two different coexisting progenitor paths (e.g., DD and SD), or from bimodality in some secondary parameter, such as the binary separation distribution, of a single explosion mechanism. Regardless, there is currently an unclear picture on the form of the DTD, even at the most coarse resolution level.

A shortcoming of the approaches described above for recovering the DTD is that they involve averaging over the galaxy population (i.e., all the SNe are assumed to come from the entire host population considered), or averaging over time (i.e., the detailed SFH of a galaxy is represented by a single “age” or simplified history for all galaxies of a certain type). Consequently, these approaches involve loss

¹ We note that diverse delay ranges have been associated in the literature with the term “prompt” — e.g., < 100 Myr (Mannucci et al. 2006); < 180 Myr (Aubourg et al. 2008); 200–500 Myr (Raskin et al. 2009b); < 350 , < 700 Myr, or < 1 Gyr (Scannapieco & Bildsten 2005). The term therefore generally labels delays of roughly a few hundred Myr. In our analysis of the Lick Observatory SN Search herein, we will define prompt SNe Ia as those with delays < 420 Myr.

of information, and potential systematic errors (e.g., due to unrepresentative simplified histories).

In this paper, the fourth in a series analysing SN rates from the Lick Observatory SN Search (LOSS), we introduce a new approach to recover the DTD, by posing DTD inversion as a discretised linear problem. In this process, we use all of the available information on the SFHs of individual galaxies, rather than averaging rates over many types of galaxies in some redshift interval, or assigning a mean star-formation-weighted age to each galaxy. In §2 below, we present the method, and in §3, we apply the method to a subsample of LOSS galaxies and their SNe. We test the method’s performance on simulated SN surveys in §4. Our results are summarised and we discuss some future prospects in §5.

2 RECONSTRUCTION OF THE SN DTD — METHOD

Consider a sample of N galaxies. The SN rate in the i th galaxy observed at cosmic time t is given by the convolution

$$r_i(t) = \int_0^t S_i(t - \tau)\Psi(\tau)d\tau, \quad (1)$$

where $S_i(t)$ is the SFR versus cosmic time of the i th galaxy (stellar mass formed per unit time), $\Psi(\tau)$ is the DTD (SNe per unit time per unit stellar mass formed), and the integration is from the Big Bang ($t = 0$) to the time of observation. For the purpose of this paper, we assume that the DTD is a universal function: it is the same in all galaxies, independent of environment, metallicity, and cosmic time — a simplifying assumption that may be invalid at some level. For example, a dependence of SN delay time on metallicity is expected in some models (e.g., Kobayashi et al. 2000). Similarly, variations in the initial mass function (IMF) with cosmic times or environment would also lead to a variable DTD, but we will again ignore this possibility in the present context.

In contrast to the averaging approaches followed in the past (see §1), we will attempt to recover the DTD by directly inverting a linear, discretized version of Eq. 1, where the detailed history of every individual galaxy or galaxy subunit is taken into account. Suppose the SFHs of the $i = 1, 2, \dots, N$ galaxies monitored as part of a SN survey are known (e.g., based on reconstruction of their stellar populations), with a temporal resolution that permits binning the stellar mass formed in each galaxy into $j = 1, 2, \dots, K$ discrete time bins, where increasing j corresponds to increasing lookback time. The time bins need not necessarily be equal, and generally will not be, since the temporal resolution of the SFH reconstruction degrades with increasing lookback time. For the i th galaxy in the survey, the stellar mass formed in the j th time bin is m_{ij} . The mean of the DTD over the j th bin (corresponding to a delay range equal to the lookback-time range of the j th bin in the SFH) is Ψ_j . Then the integration in Eq. 1 can be approximated as a sum,

$$r_i \approx \sum_{j=1}^K m_{ij}\Psi_j, \quad (2)$$

where r_i , the SN rate in a given galaxy, is measured at a particular cosmic time (e.g., corresponding to the redshift of the particular SN survey). Given a survey of N galaxies,

each with an observed SN rate, r_i , and a known binned SFH, m_{ij} , one could, in principle, algebraically invert this set of linear equations and recover the best-fit parameters describing the binned DTD: $\Psi = (\Psi_1, \Psi_2, \dots, \Psi_K)$.

In practice, on human timescales SNe in a given galaxy are rare events ($r_i \ll 1 \text{ yr}^{-1}$). Supernova surveys therefore monitor many galaxies, and record the number of SNe discovered in every galaxy. For a given model DTD, Ψ , the i th galaxy will have an expected number of SNe

$$\lambda_i = r_i t_i, \quad (3)$$

where t_i is the effective visibility time (often called the “control time”) during which a SN of a particular type would have been visible (given the actual on-target monitoring time, the distance to the galaxy, the flux limits of the survey, and the detection efficiency). Since $\lambda_i \ll 1$, the number of SNe observed in the i th galaxy, n_i , obeys a Poisson probability distribution with expectation value λ_i ,

$$P(n_i|\lambda_i) = (e^{-\lambda_i}\lambda_i^{n_i})/n_i!, \quad (4)$$

where n_i is 0 for most of the galaxies, 1 for some of the galaxies, and more than 1 for very few galaxies.

2.1 Maximum-likelihood DTD recovery

We now introduce a nonparametric, maximum-likelihood method to recover the DTD and its uncertainties. Considering a set of model DTDs, the likelihood of a particular DTD, given the set of measurements n_1, \dots, n_N , is

$$L = \prod_{i=1}^N P(n_i|\lambda_i). \quad (5)$$

More conveniently, the log of the likelihood is

$$\ln L = \sum_{i=1}^N \ln P(n_i|\lambda_i) = - \sum_{i=1}^N \lambda_i + \sum_{i=1}^N \ln(\lambda_i^{n_i}/n_i!), \quad (6)$$

where obviously only galaxies hosting SNe contribute to the second term. The best-fitting model can be found by scanning the parameter space of the vector Ψ for the value that maximizes the log-likelihood. This procedure naturally allows restricting the DTD to have only positive values, as physically required (a negative SN rate is meaningless).

The covariance matrix C_{jk} of the uncertainties in the best-fit parameters can be found (e.g., Press et al. 1992) by calculating the curvature matrix,

$$\begin{aligned} \alpha_{jk} &= \frac{1}{2} \frac{\partial^2 \ln L}{\partial \Psi_j \partial \Psi_k} = \sum_{i=1}^N \frac{\partial[\ln P(n_i|\lambda_i)]}{\partial \Psi_j} \frac{\partial[\ln P(n_i|\lambda_i)]}{\partial \Psi_k} \\ &= \sum_{i=1}^N t_i^2 (n_i/\lambda_i - 1)^2 m_{ij} m_{ik}, \end{aligned} \quad (7)$$

and inverting it,

$$[C] = [\alpha]^{-1}. \quad (8)$$

Because the values of the DTD are constrained to be positive, if the maximum-likelihood value of a DTD component, Ψ_j , is close to zero, the square root of its variance, $\sqrt{C_{jj}}$, will not represent well its 1σ uncertainty range. An alternative, more reliable, procedure is to perform a Monte-Carlo

simulation in which many mock surveys are produced, each having the same galaxies, SFHs, and visibility times as the real survey, and having expectation values λ_i based on the best-fit DTD, but with the number of SNe in every galaxy, n_i , drawn from a Poisson distribution according to λ_i . The maximum-likelihood DTD, Ψ , is found for every realization. From the distribution of the values of every component, Ψ_j , over all the realizations, one can estimate the range encompassing, say, $\pm 34\%$ of the cases.

The above approach for recovering the DTD has several advantages over previous methods. First, all of the known information in the survey is included in the analysis in a statistically rigorous way, including the fact that many (usually most) of the galaxies did not host any SNe. Furthermore, the calculation is easily generalized to cases where the galaxies are not all at the same distances (e.g., combinations of surveys done at different redshifts) – one simply needs to use the appropriate SFH bins and visibility times for every galaxy. In fact, assuming that the DTD is a universal function, it is straightforward to include in a single analysis the data from completely disparate SN surveys. For example, one could combine the results of normal SN surveys with unconventional SN “surveys,” in which the SN rate is measured based on SN remnants in small subunits of a few nearby galaxies (Maoz & Badenes 2010).

The number and resolution of the time bins used in the analysis will naturally depend on the quality of the data. Larger numbers of observed SNe, N_{tot} , as well as better data on the parent stellar populations (integrated colors and/or spectra), will permit a larger number of independent SFH and DTD time bins, and will thus improve the time resolution of the recovered DTD. We quantify this in §4, below.

3 APPLICATION TO THE LOSS-SDSS SAMPLE

We now apply our method to the SN survey data obtained by considering all LOSS galaxies with SFHs based on spectroscopy from the Sloan Digital Sky Survey (SDSS). First, we summarize briefly the essentials of each of these surveys and of the sample resulting from their intersection.

3.1 The Lick Observatory SN Search

The LOSS is an ongoing survey for SNe in a sample of $\sim 15,000$ nearby (redshift $z < 0.05$) galaxies, conducted with the Katzman Automatic Imaging Telescope (KAIT) at Lick Observatory (Li et al. 2000; Filippenko et al. 2001; Filippenko et al. 2010). KAIT is a fully robotic telescope whose control system checks the weather and performs observations with a dedicated CCD camera without human intervention. The data are automatically processed through an image-subtraction pipeline, and candidate SNe are flagged and visually inspected. The promising SN candidates are re-observed and the confirmed SNe are reported to the Central Bureau of Astronomical Telegrams.

A series of papers (Filippenko et al. 2010; Leaman et al. 2010; Li et al. 2010a,b) present the details and first results on the rates of SNe in the local Universe based on LOSS, using a sample of 1036 SNe discovered in more than 2 million observations between March 1998 through the end of

2008. This is the largest and most homogeneous set of SN statistics ever assembled for the determination of local SN rates. Filippenko et al. (2010) describe the instrumentation and the details of the SN survey. Leaman et al. (2010, Paper I in this series) present the control-time calculation for the galaxies in the sample, for SNe of different types and their luminosity functions (LFs), and details of the galaxy and SN samples used in the rate calculations. Monte-Carlo simulations are used to determine the limiting magnitude and the SN detection efficiency in each LOSS search image.

Li et al. (2010a, Paper II in the series) discuss the observed SN LF using a volume-limited sample ($D < 60$ Mpc for CC SNe and $D < 80$ Mpc for SNe Ia) of 177 SNe, each with detailed spectroscopic classification and peak magnitude from dedicated photometric follow-up images or unfiltered survey images. These observed LFs solve two issues that have plagued historical SN-rate calculations – the intrinsic luminosity distribution of SNe and the host-galaxy extinction. Finally, Li et al. (2010b, Paper III) combine all of the above ingredients, obtaining control times for different types of SNe and for each galaxy, based on its monitoring history, the observed LFs, and the limiting magnitudes and detection efficiencies of the search images. These are used to derive SN rates for SNe of different types, as a function of various galaxy properties.

3.2 VESPA star-formation histories of SDSS galaxies

The SDSS (York et al. 2000) is a survey of $\sim 10^4$ deg² of the north Galactic cap, consisting of imaging in five photometric bands (u, g, r, i, z), and $3''$ -aperture fibre spectroscopy of $\sim 10^6$ targets, mostly galaxies, with $r \lesssim 18$ mag. Tojeiro et al. (2009) performed spectral synthesis modeling of all galaxy spectra in the SDSS using their VESPA code (Tojeiro et al. 2007). VESPA uses all of the available absorption features, as well as the shape of the continuum, to deconvolve the observed spectra and obtain an estimate of the SFH. In order to recover the maximum amount of reliable information, the number of time bins used is variable, and depends on the quality of the data on each galaxy. At the highest resolution, VESPA uses 16 age bins, logarithmically spaced between 0.002 Gyr and $t_0 = 13.7$ Gyr, the age of the Universe. When data do not have sufficiently high signal-to-noise ratio for a fully resolved reconstruction, pairs of adjacent time bins are averaged. This process may be repeated down to the last two remaining bins. In the end, the SFH of every galaxy is computed using a different set of time bins.

VESPA masses are calculated assuming a Kroupa (2007) IMF; all of our results will therefore include this assumption implicitly. Bell et al. (2003) have shown that the Kroupa IMF gives a similar total stellar mass to that of a “diet Salpeter” IMF, obtained by multiplying by 0.7 the total mass of the original Salpeter (1955) IMF, to account for the reduced number of low-mass stars. Thus, our results will be comparable to other SN rate studies, such as Mannucci et al. (2005, 2006), that have assumed the diet-Salpeter IMF.

3.3 The LOSS-SDSS-VESPA sample

With the kind assistance of R. Tojeiro, we have derived VESPA SFHs for all of the LOSS galaxies that have SDSS

spectroscopy. Our main sample of LOSS galaxies with VESPA SFHs consists of 3505 galaxies that hosted 201 SNe, among them 82 SNe Ia, 93 SNe II, and 26 SNe Ibc (see Filippenko 1997 for a review of SN types; here we classify SNe Ib and Ic as “Ibc”). An alternative sample, using a different VESPA dust model (see below), has slightly different numbers: 3508 galaxies hosting 202 SNe, among them 81 SNe Ia, 94 SNe II, and 27 SNe Ibc. These numbers of SNe are consistent with those expected based on the fraction of the total LOSS visibility time that is in the VESPA galaxies. Other than the increase in Poisson errors due to the smaller number of SNe, the limitation of the calculation to VESPA galaxies should have no effect on our DTD reconstruction.

For the majority of these galaxies, it is practical to separate the SFHs into no more than four time bins: 0–70 Myr, 70–420 Myr, 420 Myr–2.4 Gyr, and > 2.4 Gyr. These correspond to the bins labeled 24, 25, 26, and 27 in Tojeiro et al. (2009). However, for each galaxy, the distribution of mass between the first two bins depends strongly on the particular dust model that is assumed, as well as on the spectral synthesis code that is used – Bruzual & Charlot (2003), or Maraston (2005) (R. Tojeiro, 2009, private communication). In fact, for some models, only a small fraction of the galaxies have any mass formed in the second time bin, a problem that persists at some level in other models as well. Due to this degeneracy, we have chosen to combine the first two time bins into a single bin, of 0–420 Myr. As the choice of stellar population model parameters affects the results in other time bins as well, we have used two alternative VESPA SFH reconstructions. One assumes a single dust component for each galaxy, while the other allows separate dust components for the young and the old stellar populations, effectively introducing an additional free parameter to the modeling (see Tojeiro et al. 2009, for details). Both reconstructions use the Maraston (2005) spectral synthesis models. Using these different SFH reconstructions gives some idea of the systematic errors in the DTD reconstruction arising from the uncertainty in the SFH (until now, we have treated the SFH values, m_{ij} , as error-free independent variables).

3.4 The core-collapse-SN DTD

We begin by deriving the DTD of the CC SNe in the LOSS-SDSS sample. Core-collapse SNe explode within $\lesssim 40$ Myr of star formation, and therefore their DTD should have zero amplitude on timescales much longer than this. This can provide a first test of our sample and of the DTD recovery method.

3.4.1 Full-sample core-collapse SN DTD

Figure 1 shows the reconstructed CC SN DTD, and its uncertainties from the Monte-Carlo simulations described above, for the full sample of 3505 LOSS galaxies with VESPA SFHs using a single dust parameter. The SNe in this sample consist of 93 SNe II and 26 SNe Ib and Ic. Since SNe II and SNe Ibc have different visibility times, we have derived the DTD for each subsample separately, added the resulting DTD amplitudes in the corresponding bins, and added the uncertainties in quadrature. Like the SFHs, the DTD in Figure 1 has three time bins, corresponding to

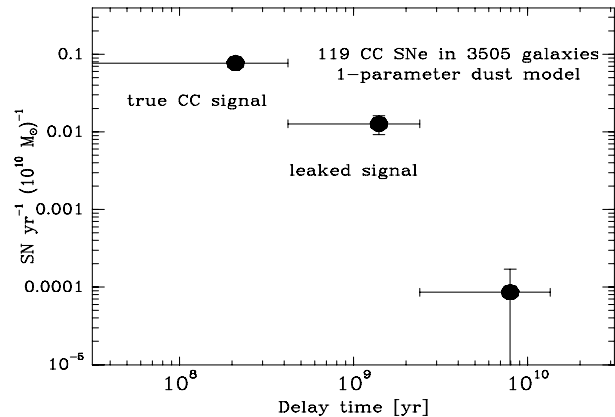


Figure 1. Best-fit delay-time distribution found for the full LOSS-SDSS core-collapse SN sample using the VESPA SFH reconstruction with a single dust parameter. Points mark the best-fit values for each time bin, whose range is indicated by the horizontal error bars. Vertical error bars show the most likely 68% range. Note the nonzero amplitude of the DTD in the delayed bins, due to “leakage” from the prompt bin resulting from incorrect characterization of the full stellar populations of the galaxies by the limited aperture of the SDSS spectra.

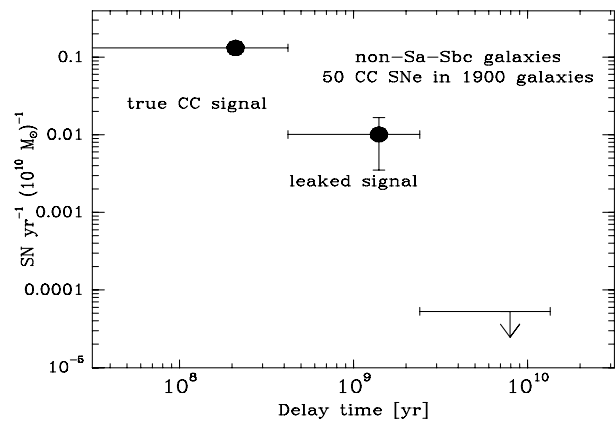


Figure 2. Same as Fig. 1, but using a subsample obtained by culling the LOSS-SDSS sample of all galaxies of Hubble type Sa–Sbc, for which SDSS fibre spectra do not represent well the full stellar population of a galaxy. Symbols are as in Fig. 1. Note the enhanced ratio of rates between the first and second bins, due to reduced leakage. The best-fit rate in the third bin is zero, and its 95% confidence upper limit is marked. Nevertheless, the leakage is not eliminated completely, and the statistical errors are larger because of the reduced sample.

< 420 Myr (“prompt” SNe), 420 Myr – 2.4 Gyr (“medium delay” SNe), and > 2.4 Gyr (“delayed” SNe). The best-fit values and the uncertainties for these DTDs, as well as additional ones discussed below, are listed in Table 1.

The prompt, < 420 Myr bin, in which all CC SNe should reside, indeed has a clear, $> 7\sigma$ signal². However, there is

² We will henceforth use the phrasing “ $X\sigma$ signal” to denote the number of -1σ (-34%) errors by which a best-fit DTD level is above zero. Naturally, in some cases this will not correspond to

Table 1. Summary of DTD reconstructions

| Sample | N_{gal} | N_{SN} | Ψ_1 0–0.42 Gyr | Ψ_2 0.42–2.4 Gyr | Ψ_3 2.4–14 Gyr | N_{SN}/M |
|---------------|------------------|-----------------|------------------------|--------------------------|------------------------|-----------------------|
| (1) | (2) | (3) | (4) | (5) | (6) | (7) |
| CC SNe | | | | | | |
| Full CC | 3505 | 119 | 770 ± 100 | 127 ± 35 | 8.6 ± 8.5 | 0.00585 ± 0.00085 |
| No Sa–Sbc | 1900 | 50 | 1320 ± 230 | 101 ± 66 | < 5.3 | 0.00750 ± 0.00150 |
| $D < 100$ Mpc | 1951 | 92 | 1037 ± 146 | 192 ± 62 | < 4.3 | 0.00920 ± 0.00130 |
| $D < 65$ Mpc | 851 | 45 | 1430 ± 340 | 223 ± 165 | < 13.4 | 0.01040 ± 0.00360 |
| SNe Ia | | | | | | |
| Full, 1-dust | 3505 | 82 | 84^{+54}_{-39} | 37^{+22}_{-14} | $2.6^{+0.8}_{-0.6}$ | 0.00137 ± 0.00032 |
| Full, 2-dust | 3508 | 81 | 26^{+16}_{-20} | 20^{+12}_{-12} | $3.3^{+0.8}_{-0.5}$ | 0.00086 ± 0.00024 |
| No Sa–Sbc | 1900 | 49 | 136^{+110}_{-56} | 55^{+40}_{-28} | $3.0^{+1.5}_{-0.6}$ | 0.00200 ± 0.00060 |

Column header explanations:

(1)- Sample used to derive DTD: *Full CC* – full core-collapse (types II and Ibc) SN sample with VESPA SFH reconstructions using a single-parameter dust model; *No Sa–Sbc* – sample excluding all galaxies of Hubble type Sa through Sbc, to avoid small-fibre aperture effects; *D < 100 Mpc* – core-collapse SN sample in galaxies within 100 Mpc; *D < 65 Mpc* – core-collapse SN sample in galaxies within 65 Mpc. *Full, 1-dust* – full SN Ia sample, with VESPA SFH reconstructions using a single-parameter dust model; *Full, 2-dust* – full SN Ia sample, with VESPA SFH reconstructions using a two-parameter dust model.

(2) - Number of galaxies in sample.

(3) - Number of SNe in sample.

(4-6) - DTD rates and 68% uncertainty ranges, in units of 10^{-4} SNe $\text{yr}^{-1} (10^{10} M_{\odot})^{-1}$. Upper limits, where given, correspond to a best fit of 0, and to the 95% confidence limit.

(7) - Time-integrated DTD, in units of SNe M_{\odot}^{-1} .

also a strong 3.5σ -level DTD signal in the 420 Myr–2.4 Gyr bin, where no CC explosions are expected. As we will demonstrate and quantify in §3.4.2 below, this result is due to the following systematic error. The SDSS spectra of many of the LOSS galaxies (which are relatively nearby, and hence large in angle) are dominated by the old populations in the centre of each galaxy, due to the limited $3''$ aperture size of the SDSS fibres. However, many of the CC SNe explode in the outer regions, where there is ongoing star formation that is invisible to the SDSS spectroscopy. As a result, our DTD solution mistakenly associates these CC SNe with an old population, and hence a large delay. We also note that the integrals over these two bins of the best-fit DTD are comparable: $\Psi_1 \Delta t_1 = 0.00325$ and $\Psi_2 \Delta t_2 = 0.00251$ CC SNe per M_{\odot} formed, respectively, where $\Delta t_1 = 420$ Myr and $\Delta t_2 = 1.98$ Gyr are the lengths of the time bins. Thus, about 40% of the prompt-bin signal has leaked into bin 2. It is unavoidable that the same process will distort the results for the DTD of SNe Ia in the same way.

In the third bin, > 2.4 Gyr, the best-fit amplitude is again nonzero, but only at the 1σ level, and the integral over this bin, $\Psi_3 \Delta t_3 = 9 \times 10^{-5} M_{\odot}^{-1}$, is just a few percent of the first two bins. Thus, there is little leakage of power to bin 3.

the Gaussian probability associated with $X\sigma$, either for obtaining zero given the best-fit result, or for obtaining the best-fit result given zero. We will discuss these subtleties where relevant.

3.4.2 Subsamples selected to reduce crosstalk

To understand the effect of the small-aperture SDSS fibres, and in an attempt to find a method of obtaining cleaner signals in the DTD, we have experimented with culling the galaxy sample in various ways, based on the galaxy properties. For example, we expect that much of the “leak” that we see is caused by early-type spirals, in which the spectrum of the bulge, covered by the SDSS fibre, is highly unrepresentative of the galaxy disk. In contrast, elliptical galaxies and late-type spirals both have more spatially uniform stellar populations. We have therefore derived the DTD, shown in Figure 2, for CC SNe from a subsample that excludes all LOSS galaxies with Hubble types 3 to 5 in the notation of Leaman et al. (2010), corresponding approximately to types Sa to Sbc. This reduces the sample size to 1900 galaxies, hosting 34 SNe II and 16 SNe Ibc (see Table 1). As expected, the prompt signal in Ψ_1 is strengthened by a factor 2, while Ψ_2 is reduced in amplitude. The best-fit value for Ψ_3 is reduced to 0.

Unfortunately, as seen in Figure 2 and in the numbers in Table 1, hand-in-hand with the increase/decrease in DTD amplitude of the first/second bin, the smaller SN numbers in the reduced sample lead to larger statistical errors. We have experimented with additional sample culling methods. For example, the SDSS database gives, for each galaxy, the magnitude in each photometric band in an aperture of the size of the spectrograph fibre, and various measures of the total magnitude of the galaxy. One can thus select to include in the DTD analysis only galaxies with no or weak radial color gradients. Additional or alternative cuts can be made based on galaxy size, distance, or fraction of total light within the fibre aperture (i.e., degree of concentration). We

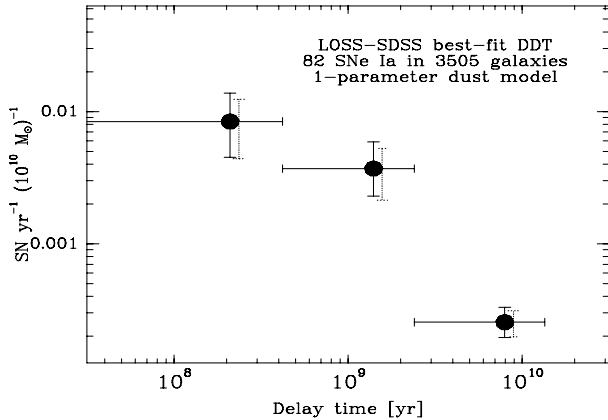


Figure 3. Best-fit SN Ia delay-time distribution found for the LOSS-SDSS sample using the VESPA SFH reconstruction with a single dust parameter. Points mark the best-fit values for each time bin, whose range is indicated by the horizontal error bars. Solid vertical error bars show the most-likely 68% range, based on Monte-Carlo simulations that use the best-fit DTD values. Dashed vertical error bars (slightly shifted to the right, for clarity) show the Gaussian 1σ errors from calculation of the covariance of the parameters. The Gaussian errors are symmetric about the best fit, but appear asymmetric in the plot because of the logarithmic scale.

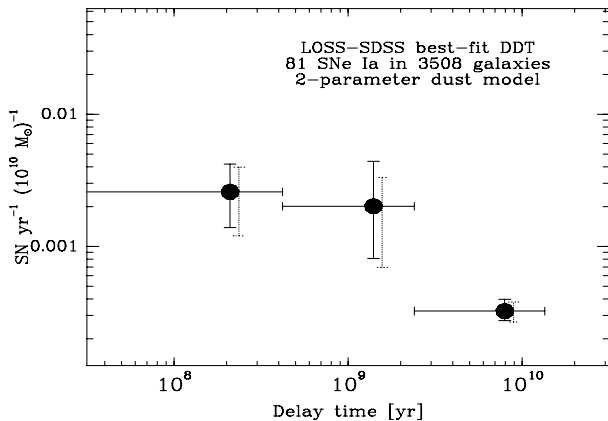


Figure 4. Same as Fig. 3, but using a VESPA SFH reconstruction permitting separate dust components for the young and the old stellar populations of each galaxy.

find that, as with the case of the selection (above) according to Hubble type, the more stringent the selection, the lower the leak out of the first bin in the CC SN DTD. At the same time, the lowered sample size increases the statistical errors.

3.5 The SN Ia DTD

Keeping in mind the systematics evidenced in the case of the CC SNe, we now proceed to derive the DTD for the SNe Ia in the sample.

3.5.1 Full-sample SN Ia DTD, one-parameter dust model

Figures 3–4 show the reconstructed SN Ia DTDs, and their uncertainties, for the LOSS-SDSS sample, using the two different VESPA-based SFHs. As for the CC SNe, the best-fit values and the uncertainties for these DTDs are listed in Table 1.

In the DTD based on the SFHs with a one-parameter dust model, we obtain, in the “prompt” (< 420 Myr) bin, a best-fit value of $\Psi_1 = 0.0084^{+0.0054}_{-0.0039}$ SNe $\text{yr}^{-1} (10^{10} M_\odot)^{-1}$. (In other words, following a δ -function starburst that forms a stellar mass of $10^{10} M_\odot$, the mean SN Ia rate in this stellar population over the first 420 Myr will be $0.0084^{+0.0054}_{-0.0039}$ SNe yr^{-1} .) This result implies a $> 2\sigma$ detection of a prompt SN Ia component. As before, the uncertainties we quote are the statistical errors, as derived from the most probable $\pm 34\%$ range in Monte-Carlo simulations, using the best-fit values as input. A model with the above best-fit value of Ψ_1 as input yields a recovered Ψ_1 of 0 in fewer than 3% of the Monte-Carlo realizations. Conversely, a model with an input value of $\Psi_1 = 0$ yields a recovered $\Psi_1 \geq 0.0084$ (in the same units as before) in $< 0.2\%$ of the realizations. Models with an input value of $\Psi_1 \leq 0.0031$ yield a recovered $\Psi_1 \geq 0.0084$ in $< 5\%$ of Monte-Carlo realizations. Thus $\Psi_1 = 0.0031$ can be considered a 95%-confidence lower limit on the level of a prompt SN Ia component.

As another test of the presence of a prompt SN Ia component, we have forced $\Psi_1 = 0$ in the DTD reconstruction. Compared to the previous result, the log of the likelihood of the best-fit model decreases by 3.0. Since $2\Delta \ln L \approx \Delta \chi^2$, this indicates that a prompt component in the model improves the fit to the data at the 2.5σ level. Thus, this test supports, at the $\sim 99\%$ confidence level, the existence of SNe Ia that explode within 420 Myr after star formation.

Since the uncertainties here are larger than was the case with the CC SN DTD, we can use this case to compare the adequacy of the errors calculated directly using the covariance-matrix formalism to those from the Monte-Carlo simulations. From Figs. 3–4, we see that the analytic 1σ errors generally match well the errors estimated from the simulations. From these simulations, we also find that the likelihood of the best-fit model is attained in at least 10% of simulated trials, indicating that the best-fit model is acceptable in an absolute sense as well.

The mean rate found above in the first bin, Ψ_1 , can be translated into an equivalent value of the “ B ” parameter (Scannapieco & Bildsten 2005), the constant of proportionality between the SFR and the “prompt” SN Ia rate (i.e., B is the number of prompt SNe per unit stellar mass formed). Multiplying Ψ_1 by 420 Myr to integrate over the bin, and dividing by 10^{10} to express the result per solar mass, the best-fit DTD value in the prompt bin implies $B \approx (3.5 \pm 1.7) \times 10^{-4} M_\odot^{-1}$ (or $B < 8 \times 10^{-4} M_\odot^{-1}$ for the 2σ upper limit). This is several times lower than the values of B estimated by studies that compare the SN Ia rate per unit mass and the SFR in blue, vigorously star-forming galaxies [see recent summary and intercomparison in Maoz (2008); observables that are quoted there per unit stellar mass formed need to be divided by 0.7 to convert from the pure Salpeter IMF assumption to the low-mass-truncated or “diet” IMFs considered here – Kroupa (2007) or, equivalently in terms of integrated mass, diet-Salpeter

(Bell et al. 2003); see §3.2]. Such studies have usually found values of $B = (1 - 3) \times 10^{-3} M_{\odot}^{-1}$ (an exception is the value $B = (3.9 \pm 0.7) \times 10^{-4} M_{\odot}^{-1}$ found by Sullivan et al. 2006).

As we showed in §3.4.2 above, at least part of this discrepancy must be due to the limited $3''$ aperture size of the SDSS fibres. Just as our CC SN DTD solution mistakenly associated CC SNe with an old population, and hence a large delay, it will do so for prompt SNe Ia that are associated with star-forming regions in the outer parts of a galaxy, outside the bulge-light-dominated fibre aperture. In fact, the leak should be comparable to the 40% effect we saw for CC SNe. Thus, the true Ψ_1 level in Figure 3 is likely about double the derived, “leaky” one, and thus coincident, within the uncertainties, with the B -parameter values found by other studies, above. By the same token, our $> 2\sigma$ significance on the detection of a prompt component is a lower limit.

Another contribution to the difference between the time-integrated Ψ_1 value and published B values may be that the B parameter found from SN rate measurements in galaxies with the highest SFRs are tracing a SN Ia population with an even smaller delay time, of $\lesssim 100$ Myr (Mannucci et al. 2005, 2006; Aubourg et al. 2009). The fact that our first time bin goes up to 420 Myr could then lead to a dilution of Ψ_1 , due to its being averaged over the lower rates at these larger delays.

Turning to the later bins in the recovered SN Ia DTD, the intermediate-delay bin of 420 Myr to 2.4 Gyr has a signal of $\Psi_2 = 0.0037_{-0.0014}^{+0.0022}$ SNe yr $^{-1}(10^{10} M_{\odot})^{-1}$. Although the uncertainty is still relatively large, there is a $\sim 2.5\sigma$ DTD signal above zero in this bin. Naturally, some or all of this signal could be due to the “leak” from the prompt bin, discussed above. Based on the observed 40% leak in the CC SN DTD, $\sim 20\%$ of the Ψ_2 signal could be leaked from Ψ_1 .

Finally, the last DTD bin, > 2.4 Gyr, has the clearest signal, $\Psi_3 = (2.55_{-0.60}^{+0.75}) \times 10^{-4}$ SNe yr $^{-1}(10^{10} M_{\odot})^{-1}$. At face value, this implies a $\sim 4\sigma$ detection of a population of SNe Ia with large delays. The “ A ” parameter defined by Scannapieco & Bildsten (2005) was meant to measure the SN Ia rate per unit mass in an old population that has no ongoing star formation. Actually, SN Ia rates are expected to vary significantly among quiescent stellar populations of different ages, and therefore like the B parameter, A will depend on the ages of the stellar populations probed by a SN survey. Indeed, the typical values found for the A parameter have been in the range $A \approx (2 - 10) \times 10^{-4}$ SNe yr $^{-1}(10^{10} M_{\odot})^{-1}$ (see compilation in Maoz 2008). However, Ψ_3 is the rate per unit mass *formed*. The published rates in old populations are a per unit of *existing* stellar mass (i.e., in stars and stellar remnants). The difference is given by the stellar mass returned to the interstellar medium via SN explosions and mass loss during stellar evolution. The fraction of returned material is an increasing function of time, and corresponds to $\sim 25\%$ after 0.1 Gyr and $\sim 50\%$ after 12 Gyr (Bruzual & Charlot 2003). Thus, for comparison to the A parameter, Ψ_3 needs to be doubled, giving a rate of $(5.1_{-1.2}^{+1.5}) \times 10^{-4}$ SNe yr $^{-1}(10^{10} M_{\odot})^{-1}$, in excellent agreement with other measurements of SN Ia rates in old populations. In principle, some or all of the Ψ_3 signal could again be the result of a leak from the prompt bin, due to the limited spatial coverage of the SDSS fibres. In practice, the time integral over the Ψ_3 rate, $\Psi_3 \Delta t_3$, is seen to be comparable to $\Psi_1 \Delta t_1$, as opposed to the few-percent leak into the

Ψ_3 bin that we found in the CC SN case in §3.4.2. This suggests that our Ψ_3 value is real and largely uncontaminated. Furthermore, examining the time integrals over the best-fit DTD in each of the bins, and attempting to correct for the leak from bin 1 to bin 2, suggests a relative contribution to the total SN Ia numbers of (prompt:medium:delayed) $\approx 2:2:1$. However, this is subject to large statistical and systematic uncertainties.

It has been known for a long time that SNe Ia can occur in early-type galaxies with little or no star formation, and hence our measurement of a significant delayed component is hardly revolutionary. However, a SN Ia in a particular early-type galaxy can always be attributed to some residual low-level star formation combined with a short SN Ia delay time. Our measurement, on the other hand, provides a statistically robust determination of the delayed component, and its level relative to the prompt components, in a population with detailed measured SFHs.

3.5.2 Full-sample SN Ia DTD, two-parameter dust model

Using the second VESPA SFH reconstruction that utilises a two-parameter dust model, the best-fit DTD values (Fig. 4 and Table 1) for the prompt, medium, and delayed components are somewhat different from those obtained with the one-parameter dust model. However, these systematic differences are smaller than the statistical uncertainties of the results quoted above. For larger SN samples with smaller statistical uncertainties, the systematic uncertainties due to SFH modeling may, however, become dominant. In what follows, we will use only the VESPA SFHs based on the first, one-parameter dust model.

3.5.3 Culled-sample SN Ia DTD

As in §3.4.2, we have repeated the DTD derivation for SNe Ia from the subsample of 1900 galaxies that excludes Hubble types Sa to Sbc. This sample hosts 49 SNe Ia. Figure 5 shows the SN Ia DTD obtained for this culled sample.

As was the case for the CC SNe in the culled sample, the prompt-bin amplitude is enhanced compared to the full sample DTD, and the medium-delay bin rate is lowered. The rate in the third bin, in contrast, is hardly changed compared to Figure 3, reconfirming the reality of that signal.

3.5.4 Comparison to DTD models

It is beyond the scope of this paper to attempt a detailed comparison of our recovered DTD to the many models that have been proposed, and to address the progenitor issue. Nonetheless, we have superimposed in Figure 5, which is our most reliable SN Ia DTD (insofar as the leakage problems are partly mitigated in it), a selection of DTDs that have appeared in the literature. Some are empirically motivated, in the sense that they were used to relate SN-rate data with star-formation measurements, using one of the methods outlined in §1. Others are more theoretically motivated, based on a progenitor scenario.

The Scannapieco & Bildsten (2005) “ $A + B$ ” model has been discussed several times above. It is not exactly a DTD, but rather a prescription for relating a SN rate to a galaxy of

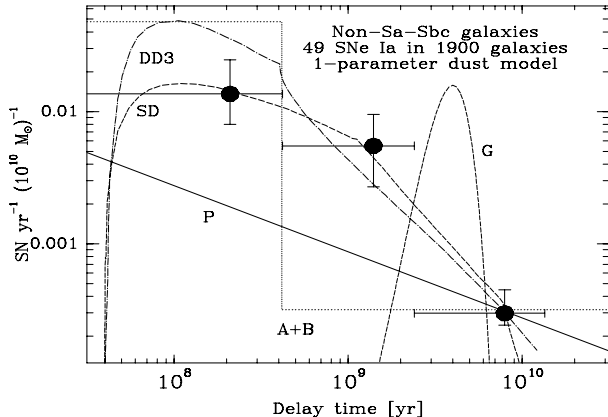


Figure 5. Best-fit SN Ia delay-time distribution found for a subsample obtained by culling the LOSS-SDSS sample of all galaxies of Hubble type Sa–Sbc, for which SDSS fibre spectra do not represent well the full stellar population of a galaxy. Symbols are as in Fig. 3. Note the enhanced ratio of rates between the first and second bins, due to reduced cross-talk. Also plotted, for comparison, are several empirically or theoretically motivated DTD models: **A+B**, representation of the Scannapieco & Bildsten (2005) “ $A + B$ ” model, plotted at the median levels of various estimates, as compiled by Maoz (2008); **G**, Gaussian DTD centred at 4 Gyr with half-width 0.8 Gyr, proposed by Strolger et al. (2004); **P**, $t^{-0.5}$ power law, suggested by Pritchett et al. (2008); **DD3**, double-degenerate “DD-Close-3” model by Greggio (2005) with $3M_{\odot}$ minimum initial mass; and **SD**, single-degenerate model of Greggio (2005), as shown by Greggio & Renzini (2008). The latter three models have been normalised to go through the best-fit observed LOSS-SDSS Ψ_3 rate for this subsample.

a given current mass and SFR. Nevertheless, we have overplotted this model in Figure 5, using the median literature values of the A and B parameters compiled by Maoz (2008). We have associated the prompt B component with the same 420 Myr bin of our DTD reconstructions, and the level to be plotted is then just the median level, $B = 2 \times 10^{-3} M_{\odot}^{-1}$ divided by this time interval. The median value for the A parameter is $A = 6 \times 10^{-4} \text{ SNe yr}^{-1} (10^{10} M_{\odot})^{-1}$, which we plot as a constant rate at times > 420 Myr, but halved to account for stellar mass loss (see above). As already noted, “ $A+B$ ” is an oversimplification, but its measured values are seen to be consistent with our DTD.

Strolger et al. (2004) and Dahlen et al. (2004) have deduced a Gaussian DTD centred at 4 Gyr with half-width 0.8 Gyr, as a best fit to their comparison of SN rates to cosmic SFH, out to $z = 1.6$. As seen in Figure 5, such a DTD is strongly at odds with our local, directly derived, DTD.

Pritchett et al. (2008) have argued for a power-law DTD form, $t^{-0.5 \pm 0.2}$, based on analysis of the Supernova Legacy Survey data. A dependence of roughly $t^{-0.5}$ is also expected simply from the formation rate of WDs, when considering the IMF and main-sequence stellar lifetimes. In Figure 5, we have plotted a $t^{-0.5}$ curve, normalised to pass through the Ψ_3 rate, which is the most robust and stable rate in our DTD reconstruction. It appears that a $t^{-0.5}$ dependence is too shallow to match our derived DTD, especially considering that Ψ_1 is likely underestimated by us, given the possibility of remaining leakage from Ψ_1 to Ψ_2 , even in our culled sample (as evidenced from the CC SN sample).

Finally, we have overplotted in Figure 5 two of the analytical models of Greggio (2005), as presented by Greggio et al. (2008), based on stellar-evolution arguments and on various parametrisations of the possible results of the complex common-envelope phases through which SN Ia progenitor systems must pass. For each of several SN Ia channels, Greggio (2005) calculates the DTDs that emerge when varying the values for the parameters describing the initial conditions, and the mass and separation distributions and limits of the systems that eventually explode. We show here one SD model and one DD model, again normalised to pass through our best-fit Ψ_3 rate.

The “DD-Close-3” label of the DD model refers to one of two possible parametric schemes used by Greggio (2005) to describe the WD separation distribution after the common-envelope phase, and to a minimum assumed initial mass of the secondary star in the binary, of $3M_{\odot}$. This DD model appears to match well our recovered DTD, especially considering that we have residual leakage problems from Ψ_1 to Ψ_2 , and hence Ψ_1 is underestimated. It is easy to see from Figure 5 that this model, after its initial rise to maximum, is essentially a broken power law. At $t \lesssim 400$ Myr, the slope is -0.5 , just like the Pritchett et al. (2008) model slope. This slope is the result of stellar-evolution lifetimes and IMF (see above). At $t > 400$ Myr, the slope is -1.3 – a slope of roughly -1 is generic to models in which the merger rate is determined by energy loss to gravitational waves (e.g., Greggio 2005; Totani et al. 2008).

The Greggio (2005) SD model also matches our recovered LOSS-SDSS DTD in Figure 5 remarkably well. It should be remembered, however, that in a full physical model, the normalisation is not a free parameter, and is dictated by the efficiency of SN Ia production from the potential progenitor population. As emphasised by Maoz (2008), and further discussed in §3.6.2, below, the efficiencies found by binary population synthesis models are at least a factor of a few, and likely an order of magnitude, lower than indicated by observed SN rates (see also Mennekens et al. 2010). Furthermore, the SD model, whose shape matches our derived DTD so nicely, has been found to be even less efficient, by yet another order of magnitude, in some studies (e.g., Tutukov & Yungelson 2002).

From this brief comparison of our recovered DTD to previous work, we conclude the following. (1) The monotonically decreasing nature of the DTD that we have found is in agreement with most previous empirical determinations and theoretical expectations, except for that of Strolger et al. (2004). (2) The decline with time of our DTD is steeper than in the Pritchett et al. (2008) model. Two of the Greggio (2005) models, SD and DD-Close-3, fit well the shape of the recovered LOSS-SDSS DTD. (3) The normalisation of full physical models to the observations has not been considered here, but it is another point at which models are challenged by these and other observations of SN rates.

3.6 The time-integrated DTD

Another interesting observable is the integral of the DTD over the age of the universe (t_0),

$$N_{\text{SN}}/M = \int_0^{t_0} \Psi(t) dt, \quad (9)$$

which gives the total number of SNe that eventually explode, per unit stellar mass formed in a short burst of star formation. We can approximate the integral in Eq. 9 with a sum over the binned DTD,

$$N_{\text{SN}}/M \approx \sum_{j=1,K} \Psi_j \Delta t_j. \quad (10)$$

The adequacy of this approximation will depend on the true form of $\Psi(t)$ and on the number of bins. From the simulations described in the next section, we find that, for declining power-law DTDs represented with three time bins, Eq. 10 typically underestimates N_{SN}/M systematically by $\sim 10 - 20\%$.

3.6.1 Core-collapse SN yield per stellar mass

If all stars with mass $> 8 M_{\odot}$ explode as CC SNe, then for CC SNe, N_{SN}/M is just the ratio of the number of stars formed above this mass limit to the total stellar mass formed, and is easily calculated to be $N_{\text{CC}}/M = 0.010 \text{ SNe } M_{\odot}^{-1}$ for the “diet” Salpeter IMF (as well as for the Kroupa (2007) IMF assumed by the the VESPA SFH reconstruction). In contrast, the integral over our reconstructed DTD of the CC SNe is $(0.00585 \pm 0.00085) \text{ SNe } M_{\odot}^{-1}$, a factor of ~ 2 lower than expected³. However, we can show that this deficit of CC SNe largely disappears in various subsamples of the LOSS-SDSS sample, and is therefore not a real effect.

For example, we have reduced the LOSS-SDSS galaxy sample by limiting the maximum galaxy distance to progressively smaller values. For each distance-limited sample, we recover the DTD. Figure 6 shows the values of N_{CC}/M we obtain by integrating over the reconstructed CC SN DTDs, for each distance limit. Several of these values are also listed in Table 1. Clearly, N_{CC}/M rises with decreasing distance, and reaches close to the theoretically expected value when the sample is limited to galaxies closer than $D \approx 65$ Mpc. From this plot we estimate the observed limiting value to be $N_{\text{CC}}/M = 0.010 \pm 0.002$.

Although a potential explanation for the dependence of N_{CC}/M on sample volume would be an increasing fraction of missing CC SNe with distance, perhaps due to mild obscuration of such SNe by dust, this is unlikely to be the correct explanation. N_{CC}/M is derived from the DTD, which takes into account the visibility time of each type of CC SN at the distance of each galaxy in the sample. The visibility time, in turn, was calculated, as described in Li et al. (2010a), using the observed LF of 87 nearby CC SNe, in which the effects of extinction are automatically included.

More likely, the decrease of N_{CC}/M with distance is another manifestation of the SDSS fibre aperture problem. At larger distances, there are fewer low-mass galaxies and late-type spirals in the LOSS sample, and more high-mass intermediate and early types. In the earlier-type galaxies, VESPA is more likely to overestimate the total galaxy mass, based on the spectrum of the bulge population probed by the SDSS aperture. Indeed, if we rederive the CC SN DTD

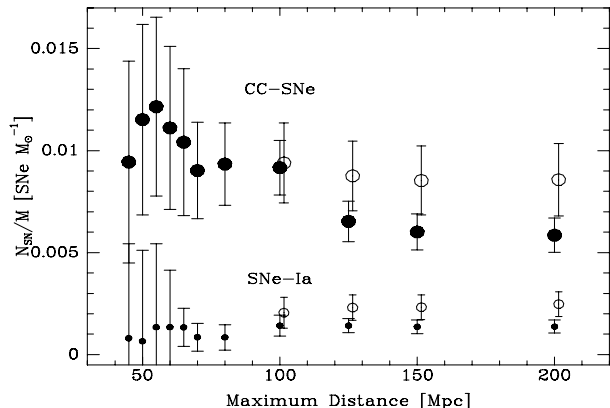


Figure 6. The time-integrated DTD, i.e., the total number of SNe produced over a Hubble time, per unit stellar mass formed, for different distance-limited galaxy subsamples. Top full symbols are for CC SNe (SNe II plus SNe Ibc), bottom full symbols are for SNe Ia. Top empty symbols are for CC SNe in a subsample of galaxies with masses $< 3 \times 10^{10} M_{\odot}$. Bottom empty symbols are for SNe Ia in a subsample of galaxies with masses $< 7 \times 10^{10} M_{\odot}$. The rise in N_{CC}/M toward its theoretically expected value with decreasing maximum sample distance or with sample culling is another manifestation of the SDSS small-fibre-aperture problem. The value of N_{CC}/M at $\lesssim 65$ Mpc indicates that most stars above $8 M_{\odot}$ produce CC SNe. The constant value of N_{Ia}/M , on the other hand, shows that the systematics affecting SNe Ia are less dependent on distance. Nevertheless, culling the higher-mass galaxies from the sample increases N_{Ia}/M at all distances. The time-integrated ratio of CC SNe to SNe Ia is seen to be roughly 4:1.

and N_{CC}/M , but exclude the earlier Hubble types (as in §3.4.2), or exclude massive galaxies, the values of N_{CC}/M for the samples limited to $D < 125$ Mpc, $D < 150$ Mpc, and $D < 200$ Mpc rise significantly, and approach their $D < 100$ Mpc values. For example, we show in Figure 6 (upper empty symbols) that, if we limit the sample to galaxies less massive (based on their VESPA reconstructions) than $3 \times 10^{10} M_{\odot}$, the best-fit DTDs at those distances give $N_{\text{CC}}/M = 0.0086 \pm 0.0017$, much closer to the expected value. (Naturally, the reduced sample sizes lead to larger statistical error bars in Fig. 6.) Another indication of the nature of the effect can be seen in Table 1, where the ratio of Ψ_2/Ψ_1 , which quantifies the leak from the first to the second bin, decreases for the CC SNe as D is reduced.

The fact that a galaxy sample can be defined (the $D \lesssim 65$ Mpc sample in the above example), for which N_{CC}/M actually reaches its expected value, is important. It confirms that, indeed, the majority of stars with $> 8 M_{\odot}$ produce CC SNe. This cannot be taken for granted. Given current observational and theoretical limits, the low-mass limit for core collapse could be as high as 10 or even $11 M_{\odot}$ (see Smartt et al. 2009, and references therein). Moving the limit from 8 to $10 M_{\odot}$ would decrease the expected N_{CC}/M by about 30% (i.e., to our 2σ observed lower limit on N_{CC}/M). Raskin et al. (2008) have recently obtained a similar estimate of the lower mass limit for core collapse by matching, on the one hand, the differences in the spatial distributions of stars and SNe in spiral galaxies to, on

³ Here, the statistical error on N_{CC}/M is found using the covariance matrix $[C]$ for Ψ , and the vector of time-bin intervals $\Delta \mathbf{t} = (\Delta t_1, \Delta t_2, \dots, \Delta t_K)$, such that $\Delta(N_{\text{SN}}/M) = (\Delta \mathbf{t}[C]\Delta \mathbf{t})^{1/2}$.

the other hand, the predictions of simple stellar-population aging models.

Furthermore, in principle, a sizable fraction of high-mass stars could collapse directly to a black hole, with only a weak or null SN explosion accompanying the collapse (Kochanek et al. 2008). Our measurements of N_{CC}/M also argue against this scenario, unless the minimum mass for CC SNe is even lower than $8 M_{\odot}$. We note that these conclusions are reinforced by the fact that the discrete sum in Eq. 10 underestimates the true integral over Ψ .

3.6.2 The SN Ia yield per stellar mass

Figure 6 also shows the results of a similar analysis for the SNe Ia: the integral N_{Ia}/M over the best-fit SN Ia DTD (shown in Fig. 3 for the full sample), again as a function of the sample distance limit. We see (lower filled symbols) that there is no obvious dependence on distance, with N_{Ia}/M apparently constant at $\sim 0.00140 \pm 0.00033 \text{ SNe } M_{\odot}^{-1}$. However, if we again limit the sample in mass, for example to $< 7 \times 10^{10} M_{\odot}$, we obtain (lower empty symbols in Fig. 6) higher values, $N_{Ia}/M \approx 0.00230 \pm 0.00060 \text{ M}_{\odot}^{-1}$. The systematics of the masses of the SN Ia host galaxies, while present, are apparently less dependent on distance than those of the CC SN hosts.

These values of N_{Ia}/M are also of interest. As already noted above, previous studies have found, just for the prompt SN Ia component embodied in the B parameter, values of $B = (1 - 3) \times 10^{-3} M_{\odot}^{-1}$. We note that the B parameter, like N_{Ia}/M , relates to the stellar mass *formed*. Mannucci et al. (2006) obtained an empirical DTD based on the observations described by Mannucci et al. (2005) and Della Valle et al. (2005). Their time-integrated SN rate is $0.0013 \text{ SNe } M_{\odot}^{-1}$. However, this rate is per unit of *existing* stellar mass, after assuming a fraction of recycled gas of 0.30 as an average among populations of different ages (Bruzual & Charlot 2003). Accounting for this factor, the Mannucci et al. (2006) result corresponds to $\sim 0.0010 \text{ SNe } M_{\odot}^{-1}$ of *formed* stars, similar to the values measured here.

As discussed at length by Maoz (2008), N_{Ia}/M is one of several observables that can be related directly to the fraction η of stars in some initial mass range $[m_1, m_2]$ that eventually explode as SNe Ia:

$$\eta = \frac{N_{Ia}}{M} \frac{\int_{0.1}^{100} m(dN/dm)dm}{\int_{m_1}^{m_2} (dN/dm)dm}, \quad (11)$$

where dN/dm is the IMF. For the ‘‘diet Salpeter’’ IMF (which, again, gives results similar to the Kroupa IMF assumed by the VESPA SFH reconstruction), and an initial mass range of 3–8 M_{\odot} , often considered for the primary stars of SN Ia progenitor systems, the ratio of the two integrals equals 33. Adopting the higher value of N_{Ia}/M we have found in the culled sample, under the assumption that it is more robust against the fibre-aperture effect, we obtain $\eta = 7.6 \pm 2.0\%$. This is in agreement with the results of Mannucci et al. (2006), who found $\eta = 4.3\%$ for these parameters. As noted by Maoz (2008), the consistently high values of the exploding fraction, η , derived from several different observables, may constitute a problem for current progenitor models.

Interestingly, in galaxy clusters, Maoz et al. (2010)

have estimated a time-integrated number of SNe Ia per present-day stellar mass of $0.012 \text{ SNe } M_{\odot}^{-1}$. This estimate is based on the observed ratio of total mass of iron (both in stars and in the intracluster medium) and the mass in stars. For an IMF with a standard high-mass end, the present-day mass observed in stars is related to the number of CC SNe, whose contribution to the iron mass can, in turn, be estimated and subtracted. The remaining iron mass is then due to the SNe Ia. Multiplying by 0.5 to convert to formed mass, rather than present mass, this gives $N_{Ia}/M = 0.006 \text{ SNe } M_{\odot}^{-1}$. Maoz et al. (2010) show that, given the uncertainties in observed cluster properties, this number could decrease by perhaps a factor of 0.6 at most, to $N_{Ia}/M = 0.0036 \text{ SNe } M_{\odot}^{-1}$. This is still at least a factor of 1.5 greater than, but marginally consistent with, the $N_{Ia}/M = 0.0023 \pm 0.0006 \text{ SNe } M_{\odot}^{-1}$ that we have found here based on LOSS.

The cluster-based value of N_{Ia}/M may be evidence for early enrichment of clusters by CC SNe from a top-heavy IMF. These CC SNe from massive stars, which left no traces in the form of low-mass relatives, would have then produced the bulk of the iron mass in clusters. Alternatively, the large iron mass in clusters could have indeed come from SNe Ia, but this would imply a more efficient production of SNe Ia in cluster environments. Intriguingly, Sharon et al. (2007), Mannucci et al. (2008), and Graham et al. (2008) have all found evidence for SN Ia rates enhanced by factors of a few in cluster galaxies, compared to field early-type galaxies.

3.6.3 The ratio of CC SNe to SNe Ia

From the ratio of the time-integrated DTDs, N_{CC}/M and N_{Ia}/M (using the value of N_{CC}/M at $D \lesssim 70 \text{ Mpc}$ for which the CC SN counts are fairly complete, but for which the errors are not excessively large because of the limited sample size, and N_{Ia}/M from the low-mass sample, see above), the time-integrated ratio of CC SNe to SNe Ia is $N_{CC}/N_{Ia} = 4_{-1.5}^{+3}$. If we force the value of $N_{CC}/M = 0.01$ expected from a diet-Salpeter IMF with a low-mass CC limit of $8 M_{\odot}$, the allowed range in the ratio shrinks to $N_{CC}/N_{Ia} = 4_{-0.7}^{+2}$. We note that the ratio of time-integrated DTDs is distinct from the observed ratio of *current rates*, which is measured to be about 3:1 in local surveys (Mannucci et al. 2005; Li et al. 2010a). The ratio of current rates depends on the summed SFH of the galaxies in the volume. It can be arbitrarily high for very young, star-forming populations (in which few SNe Ia have had time to form yet) to zero for old, inactive populations (with no CC SNe). In contrast, the ratio of the time-integrated DTDs, like the DTDs themselves, is independent of SFH, and intrinsic to the stellar-evolution processes that lead to SNe.

The ratio N_{CC}/N_{Ia} of course equals $(0.01 M_{\odot}^{-1})/(N_{Ia}/M)$, for the diet Salpeter IMF and the said lower limit for CC SNe, and thus the cluster-based lower limit of $N_{Ia}/M > 0.0036 \text{ SNe } M_{\odot}^{-1}$ (Maoz et al. 2010), discussed above, implies $N_{CC}/N_{Ia} < 2.8$, and possibly even 1:1. De Plaa et al. (2007), comparing cluster element abundances to theoretical SN element yields, have deduced an integrated CC SN to SN Ia ratio of 1:1. On the other hand, the observational uncertainties are such that a time-integrated CC SN to SN Ia ratio of roughly 3:1, despite

some tension, is consistent both with cluster measurements and with the LOSS data we have analysed here.

4 TESTS ON SIMULATED SAMPLES

To test our DTD recovery procedure and examine its performance on different kinds of input datasets, we have repeated the Monte-Carlo mock survey generation described in §2, above, using the LOSS-SDSS galaxy sample and its VESPA-based SFHs (with one dust parameter). However, rather than inputting the best-fit DTD from the inversion of the real data, we can choose other model DTDs and convolve those DTDs with m_{ij} according to Eq. 2–3, or we can change the sample properties in additional ways, as described below. Using the actual LOSS galaxy SFHs and visibility times (as opposed to, for example, random SFHs and visibility times) makes for a more realistic simulation. As before, the number of SNe found in each galaxy in each mock survey is drawn from a Poisson distribution with expectation value λ_i . The different-shaped DTDs which can be input and recovered can also be scaled up or down to produce a larger or smaller total number of SNe in the mock survey (or, equivalently, the visibility times, t_i , can be scaled up or down). In these simulations, the SFHs are assumed to be error-free independent variables, and are used both for creating the mock samples and deriving their DTD. Therefore, these simulations will not display the “leakage” between bins that we have encountered with the LOSS-SDSS sample, nor other problems due to systematic or random errors in the SFHs of the galaxies.

From our simulations, we find that the distribution of output DTD amplitudes is centered on the input DTD values, meaning that the method reliably recovers the input DTD with little bias. Nonetheless, for low DTD amplitudes combined with large uncertainties (due to small SN numbers, see below), there can be some “pile-up” in the distribution at zero amplitude, as a result of the positivity constraint of the DTD. Thus, obtaining a zero amplitude for a bin in the DTD reconstruction can happen, even when in reality the amplitude is nonzero but low, and the number of SNe in the survey is small.

We find that the relative uncertainty in the DTD amplitude in the j th bin scales roughly as one would expect from Poisson statistics, considering the number of SNe that contribute to every bin in the DTD. For example, with three time bins, the relative error in the first bin of the DTD is

$$\frac{\Delta\Psi_1}{\Psi_1} \approx \left(N_{\text{tot}} \frac{\sum_i m_{i,1}\Psi_1}{\sum_i m_{i,1}\Psi_1 + \sum_i m_{i,2}\Psi_2 + \sum_i m_{i,3}\Psi_3} \right)^{-1/2}. \quad (12)$$

For a survey with a fixed total number of SNe, N_{tot} , there will thus be a tradeoff in the analysis between DTD accuracy and resolution. The uncertainties do not depend on the number of galaxies monitored, and thus a brief-duration survey of many galaxies and a long-duration survey of few galaxies are equivalent, as long as they produce the same total number of SNe.

Figure 7 examines the quality of the reconstruction as the number of time bins is varied between three and five. Here, we have assumed a survey with 15,000 galaxies and ~ 370 SNe, similar to the full LOSS SN Ia sample, if all

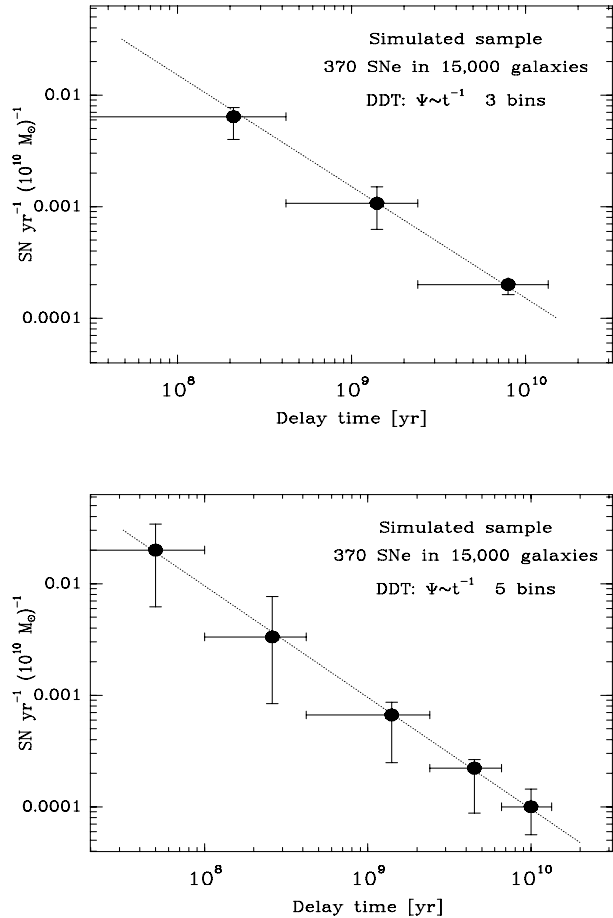


Figure 7. DTD recovered using three or five bins from a mock sample of 15,000 galaxies hosting 370 SNe Ia, the numbers characterising the full LOSS sample. The input DTD is a t^{-1} power law (dashed line). Points are plotted at the value of the input binned DTD, and error bars show the ranges that include 68% of the recovered best-fit solutions in repeated random realizations of SN surveys on the mock sample.

galaxies in it had SFH reconstructions available. To produce this large mock sample, we simply clone several times the 3505 SFHs and visibility times of the LOSS-SDSS sample, with its three time bins. To obtain a sample with five time bins in each galaxy’s SFH, we have split, in this example, the first SFH bin into two bins: a 0–100 Myr bin and a 100–420 Myr bin. The stellar mass in each sub-bin was randomised by $\pm 50\%$ around the mass value corresponding to the relative time fractions. (Such randomisation is essential, as otherwise the m_{ij} are no longer independent variables.). Similarly, we further split the last bin into two bins, corresponding to 2.4–6.5 Gyr and 6.5–13.5 Gyr. For the DTD in these simulations, we have taken a $\Psi(t) \propto t^{-1}$ dependence (which is roughly generic to DD models; see §3.5.4, above), scaled so as to give the desired total number of SNe using the LOSS visibility times. The simulations show that surveys with several hundred SNe enable reasonably good DTD recovery in terms of both accuracy and temporal resolution. Specifically, Figure 7 demonstrates that already-existing SN surveys, and LOSS in particular, have the power to measure reliably the SN Ia DTD, if the SFHs could be estimated in

a comprehensive and unbiased way for the full sample of $\sim 15,000$ galaxies. We briefly discuss the prospects for this in the concluding section, below.

We have gauged the effect of the time binning on the time integral over the DTD, N_{SN}/M , as approximated in Eq. 10. To do this, we create mock samples using large numbers of bins in the SFH and the DTD. The mock samples also have a large number of SNe in order to minimise the statistical error and isolate the systematic effect due to the binning. We then rebin the SFHs of the sample into the same three coarse time bins we have used for the LOSS-SDSS analysis, and we recover the DTD binned into those same three time intervals. Finally, we compare the integrals N_{SN}/M over the input DTD and the recovered DTD. We find that the N_{SN}/M of the recovered DTD systematically underestimates the input N_{SN}/M by 10–20%, with the larger values for input DTDs that rise more steeply at small delays. This systematic error is comparable to the statistical errors in N_{SN}/M we have found for the LOSS-DTD sample. Larger SN samples will naturally allow finer temporal binning of the DTD, reducing this systematic effect.

5 CONCLUSIONS AND OUTLOOK

We have presented a method to recover the SN DTD by jointly analysing SN survey data and reconstructed SFHs of the individual galaxies in a survey, while accounting for the small-number, Poisson-statistical nature of SN events in those individual galaxies. Our method is an improvement over previous ones in that it uses the full information contained in the data and avoids unnecessary averaging. The method is based on casting the expected SN numbers in each galaxy in the survey as a set of linear equations, in which the parameters to be constrained by the data are the values of the DTD in binned time intervals. We have shown a maximum-likelihood method by which to invert those equations to recover the DTD, and demonstrated the method’s performance using simulated mock samples. We have applied the method to a sample consisting of those galaxies in the LOSS SN survey that have SDSS-VESPA SFH reconstructions, along with the SNe that these galaxies have hosted during the LOSS.

The recovered DTDs for CC SNe and SNe Ia are limited by Poisson statistics, because of the small numbers of SNe in this restricted subset of LOSS, and by systematic errors, because for many galaxies the light within the SDSS fibre aperture does not reliably represent the full stellar population of the galaxy and its SFH. Despite these shortcomings, we are able to make the following statements based on analysis of these data.

(1) A “prompt” SN Ia population, defined here as one that explodes within 420 Myr of star formation, exists at 99% confidence. This confirms the growing number of reports of such a population, at levels similar to those found here.

(2) We clearly detect, at the 4σ level, a “delayed” SN Ia population with delays in the range 2.4–13 Gyr, and a mean rate over this interval of $\Psi_3 = (2.6 \pm 0.7) \times 10^{-4}$ SNe yr^{-1} per $10^{10} M_{\odot}$ formed, or $A = (5.1 \pm 1.4) \times 10^{-4}$ SNe yr^{-1} per remaining $10^{10} M_{\odot}$ in an old population. These first two conclusions together indicate that the SN Ia DTD peaks at short delays, but extends over a broad range of delay times,

out to at least several Gyr. Progenitor models, a few of which we have briefly compared to our recovered DTD, will need to reproduce the observed numbers.

(3) The time-integrated SN Ia yield is $N_{\text{Ia}}/M = (2.3 \pm 0.6) \times 10^{-3}$ SNe per unit solar mass formed, or $(4.6 \pm 1.2) \times 10^{-3}$ SNe Ia per remaining unit solar mass in an old population. The best-fit value is a factor of 1.5–3 lower than the corresponding number in galaxy clusters, as deduced from their measured iron-to-stellar mass ratios. Although the current uncertainties can still accommodate this difference, it may indicate that clusters underwent additional enrichment by CC SNe from an early stellar population with a top-heavy IMF, or that SN Ia production is more efficient in galaxy clusters than in the field. The latter possibility has support both from direct cluster SN rate measurements and from cluster element abundance analysis. The measured time-integrated SN Ia yield also implies $\eta \approx 8\%$ for the exploding fraction among the parent population of SN Ia primaries, if assumed to come from the 3–8 M_{\odot} initial mass range.

(4) The time-integrated CC SN yield is $N_{\text{CC}}/M = (1.0 \pm 0.2) \times 10^{-2}$ SNe per unit solar mass formed. This rules out low-mass limits for CC explosions that are much above 8 M_{\odot} . Conversely, scenarios in which a significant fraction of high-mass stars end their evolution without SN explosions are excluded, unless the low-mass limit for core collapse is significantly below 8 M_{\odot} .

(5) The ratio of CC SN to SN Ia numbers from a brief burst of star formation, integrated over a Hubble time, is $(4_{-1.5}^{+3})$.

Our work points to the kinds of data that would improve upon these results. First, a larger sample of survey galaxies with spectroscopy, and hence SFHs, would obviously reduce the Poisson errors and permit better temporal resolution. As there are 14882 galaxies monitored by LOSS, obtaining spectra for most or all of them would be a large, but not impossible, task. A dedicated or partly dedicated 2–4 m-class telescope could achieve this on a few-year timescale. Long-slit spectra, drifted across the galaxy perpendicular to the slit length, would be more representative of the entire stellar population of each galaxy, largely avoiding the small-fibre-aperture problem we have encountered. Ideally, instead of long-slit spectra of the LOSS galaxies, one would obtain integral-field spectroscopy of each of these galaxies (using, e.g., an instrument such as SAURON on the William Herschel 4.2 m telescope; Bacon et al. 2001). In addition to including the full SFH of each galaxy without any aperture losses, such data, in the context of our method, would easily allow breaking up each galaxy into independent subunits, and considering the SFH of each subunit in relation to the SNe that it hosted (or, for almost all subunits, the SNe that it did not host).

It might be objected at this point, that because of the random stellar velocities in each galaxy, SN progenitor stars diffuse away from the regions where they were formed, and that this would invalidate our approach; by the time a SN Ia exploded, it would reside within a region that is completely different from the one in which its progenitor was formed. While this is true, and it would in fact invalidate a traditional “SN delay time” analysis in which a single characteristic stellar population age is assigned to a region, it is inconsequential to our current method, in which the entire SFH of the region is considered. The reason is that the same spatial diffusion affects both the progenitor population and

those stars among it that eventually explode. To see this, consider, as a toy example, a grid of 3×3 adjacent “cells” in a particular galaxy. Suppose, for example, that 500 Myr ago there was a short burst of star formation in the central cell, forming a stellar mass M , and no activity in the other cells. Suppose, further, that the SN DTD is such that the stellar population formed in the burst leads, 500 Myr later, to nine SNe over the course of a decade, which are therefore detected in this galaxy by a SN survey such as LOSS (this is admittedly a somewhat unrealistically large number of SNe, but is used here just for the sake of illustration). The galaxy has thus produced a ratio of $9/M$ SNe per unit stellar mass formed 500 Myr ago. Finally, suppose that the stellar diffusion timescale in the galaxy is such that, over the 500 Myr, the progenitors of the 9 SNe, before exploding, have drifted out of the central cell in which they were formed, and there is now, on average, one SN in each cell. However, the entire stellar population of the burst will have diffused in the same way, and therefore each cell will have $1/9$ of the 500-Myr-old population that was originally in the central cell. When we compare SN numbers to the 500 Myr-old stellar mass present today in each cell, we will see 1 SN per $M/9$ of stellar mass formed. In the DTD we derive, we will therefore still deduce the correct ratio of $9/M$ SNe per unit stellar mass formed 500 Myr earlier.

This argument holds, no matter what are the lookback times or the diffusion timescales. It also holds for arbitrarily complex SFHs, which can be viewed as linear superpositions in space and in time of toy models of the type above. If a past starburst at a certain place and time in a galaxy produces SNe that are observed in the course of a survey, the stellar population of the burst and the SNe that it produces will both diffuse in the same way. If, on the other hand, a specific burst does not produce SNe detected by the survey (because the DTD has a low amplitude at the corresponding delay), then there will be no correlation between the number of SNe per cell and the mass of stars of that age per cell. An individual cell hosting SNe may, of course, include unrelated stellar populations that did not produce those SNe, but whose stars nonetheless drifted into the cell. However, over the entire galaxy, there will be no correlation between SNe and stars of that particular age, and it is such correlations that drive the results of our DTD recovery method.

We note that for the integral-field spectroscopy approach to work, the signal-to-noise ratio of the spectra of each individual galaxy cell needs to be sufficiently high for a reliable SFH reconstruction to be obtained. In particular, the presence of old stellar populations that are superimposed on younger and more luminous stars must be detectable. Naturally, spatially resolved, medium-spectral-resolution data of such a large sample of nearby galaxies would find many additional applications, and hence such data are worth the large effort required.

Shortly before submission of this work, Brandt et al. (2010) presented a DTD reconstruction analysis of a different SN sample. Their methodology shares several elements with ours. Brandt et al. (2010) study 107 SNe Ia from SDSS-II. Like us, they use VESPA to derive SFHs for a sample of SDSS galaxies, binned into three time bins, identical to those we have chosen. Like us, they treat the DTD amplitudes in the three discrete bins as free parameters, which are determined by a maximum-likelihood procedure. However, rather

than comparing directly the presence or absence of SNe in each galaxy to the predictions of the DTD model (as we have), they use the DTD to create mock SN-host samples, and compare the mean spectrum of the mock host samples to the mean spectrum of the real host galaxies. Brandt et al. (2010) reach similar conclusions to ours, namely, significant detections of both prompt (< 420 Myr) and delayed (> 2.4 Gyr) SN Ia DTD components.

ACKNOWLEDGMENTS

We thank Rita Tojeiro for her assistance and patience with obtaining and explaining the VESPA SFHs, Jesse Leaman for his contribution to the determination of LOSS SN rates, and Keren Sharon for her help with the comparison to models. The anonymous referee is thanked for constructive comments. D.M acknowledges support by a grant from the Israel Science Foundation. LOSS, conducted by A.V.F.’s group at the University of California, Berkeley, has been supported by many grants from the US National Science Foundation (most recently AST-0607485 and AST-0908886), the TABASGO Foundation, US Department of Energy SciDAC grant DE-FC02-06ER41453, and US Department of Energy grant DE-FG02-08ER41653. KAIT and its ongoing operation were made possible by donations from Sun Microsystems, Inc., the Hewlett-Packard Company, AutoScope Corporation, Lick Observatory, the National Science Foundation, the University of California, the Sylvia & Jim Katzman Foundation, and the TABASGO Foundation.

REFERENCES

- Aubourg, E., Tojeiro, R., Jimenez, R., Heavens, A. F., Strauss, M. A., & Spergel, D. N. 2008, *A&A*, 492, 631
 Bacon, R., et al. 2001, *MNRAS*, 326, 23
 Bell, E. F., McIntosh, D. H., Katz, N., & Weinberg, M. D. 2003, *ApJS*, 149, 289
 Bogomazov, A.I & Tutukov, A.V., 2009, *Astronomy Reports*, 53, 214
 Brandt, T. D., Tojeiro, R., Aubourg, E., Heavens, A., Jimenez, R., & Strauss, M. A. 2010, arXiv:1002.0848
 Bruzual, G., & Charlot, S. 2003, *MNRAS*, 344, 1000
 Dahlen, T., et al. 2004, *ApJ*, 613, 189
 Dahlen, T., Strolger, L.-G., & Riess, A. G. 2008, *ApJ*, 681, 462
 de Plaa, J., Werner, N., Bleeker, J. A. M., Vink, J., Kaastra, J. S., & Méndez, M. 2007, *A&A*, 465, 345
 Della Valle, M., Panagia, N., Padovani, P., Cappellaro, E., Mannucci, F., & Turatto, M. 2005, *ApJ*, 629, 750
 Filippenko, A. V. 1997, *ARAA*, 35, 309
 Filippenko, A. V., Li, W., Treffers, R. R., & Modjaz, M. 2001, in *Small-Telescope Astronomy on Global Scales*, ed. W. P. Chen, C. Lemme, & B. Paczyński (San Francisco: ASP), 121
 Filippenko, A.V., et al. 2010, in preparation
 Gal-Yam, A., & Maoz, D. 2004, *MNRAS*, 347, 942
 González Hernández, J. I., Ruiz-Lapuente, P., Filippenko, A. V., Foley, R. J., Gal-Yam, A., & Simon, J. D. 2009, *ApJ*, 691, 1
 Graham, M. L., et al. 2008, *AJ*, 135, 1343
 Greggio, L. 2005, *A&A*, 441, 1055
 Han, Z., & Podsiadlowski, P. 2004, *MNRAS*, 350, 1301
 Hurley, J. R., Tout, C. A., & Pols, O. R. 2002, *MNRAS*, 329, 897
 Iben, I., Jr., & Tutukov, A. V. 1984, *ApJS*, 54, 335
 Kerzendorf, W. E., Schmidt, B. P., Asplund, M., Nomoto, K.,

- Podsiadlowski, P., Frebel, A., Fesen, R. A., & Yong, D. 2009, *ApJ*, 701, 1665
- Kobayashi, C., Tsujimoto, T., & Nomoto, K. 2000, *ApJ*, 539, 26
- Kochanek, C. S., Beacom, J. F., Kistler, M. D., Prieto, J. L., Stanek, K. Z., Thompson, T. A., & Yuuulksel, H. 2008, *ApJ*, 684, 1336
- Kroupa, P. 2007, arXiv:astro-ph/0703124
- Leaman, J., et al. 2010, in preparation
- Li, W., et al. 2000, American Institute of Physics Conference Series, 522, 103
- Li, W., et al. 2010a, in preparation
- Li, W., et al. 2010b, in preparation
- Mannucci, F., Della Valle, M., Panagia, N., Cappellaro, E., Cresci, G., Maiolino, R., Petrosian, A., & Turatto, M. 2005, *A&A*, 433, 807
- Mannucci, F., Della Valle, M., & Panagia, N. 2006, *MNRAS*, 370, 773
- Mannucci, F., Della Valle, M., & Panagia, N. 2007, *MNRAS*, 377, 1229
- Mannucci, F., Maoz, D., Sharon, K., Botticella, M. T., Della Valle, M., Gal-Yam, A., & Panagia, N. 2008, *MNRAS*, 383, 1121
- Maoz, D., & Gal-Yam, A. 2004, *MNRAS*, 347, 951
- Maoz, D. 2008, *MNRAS*, 384, 267
- Maoz, D., & Mannucci, F. 2008, *MNRAS*, 388, 421
- Maoz, D., & Badenes, C.. 2010, *MNRAS*, submitted, arXiv:1003.3031
- Maoz, D., et al. 2010, in preparation
- Maraston, C. 2005, *MNRAS*, 362, 799
- Mennekens, N., Vanbeveren, D., De Greve, J. P., De Donder, E., *A&A*, in press, arXiv:1003.2491
- Meng, X., & Yang, W. 2010, *ApJ*, 710, 1310
- Nelemans, G., et al. 2005, *A&A*, 440, 1087
- Pritchett, C. J., Howell, D. A., & Sullivan, M. 2008, *ApJ*, 683, L25
- Roelofs, G., Bassa, Voss, R., C., & Nelemans, G. 2008, *MNRAS*, 391, 290
- Nobili, S., et al. 2005, *A&A*, 437, 789
- Poznanski, D., et al. 2007, *MNRAS*, 382, 1169
- Press, W. H., Teukolsky, S. A., Vetterling, W. T., & Flannery, B. P. 1992, Cambridge: University Press, —c1992, 2nd ed.,
- Raskin, C., Scannapieco, E., Rhoads, J., & Della Valle, M. 2008, *ApJ*, 689, 358
- Raskin, C., Timmes, F. X., Scannapieco, E., Diehl, S., & Fryer, C. 2009a, *MNRAS*, 399, L156
- Raskin, C., Scannapieco, E., Rhoads, J., & Della Valle, M. 2009b, *ApJ*, 707, 74
- Rosswog, S., Kasen, D., Guillochon, J., & Ramirez-Ruiz, E. 2009, *ApJ*, 705, L128
- Ruiter, A. J., Belczynski, K., & Fryer, C. 2009, *ApJ*, 699, 2026
- Salpeter, E. E. 1955, *ApJ*, 121, 161
- Scannapieco, E., & Bildsten, L. 2005, *ApJ*, 629, L85
- Sharon, K., Gal-Yam, A., Maoz, D., Filippenko, A. V., & Guhathakurta, P. 2007, *ApJ*, 660, 1165
- Smartt, S. J. 2009, *ARA&A*, 47, 63
- Strolger, L.-G., et al. 2004, *ApJ*, 613, 200
- Sullivan, M., et al. 2006, *ApJ*, 648, 868
- Tojeiro, R., Heavens, A. F., Jimenez, R., & Panter, B. 2007, *MNRAS*, 381, 1252
- Tojeiro, R., Wilkins, S., Heavens, A. F., Panter, B., & Jimenez, R. 2009, *ApJS*, 185, 1
- Totani, T., Morokuma, T., Oda, T., Doi, M., & Yasuda, N. 2008, *PASJ*, 60, 1327
- Tout, C. A. 2005, in *The Astrophysics of Cataclysmic Variables and Related Objects*, 330, 279
- Voss, R., & Nelemans, G. 2008, *Nature*, 451, 802
- Webbink, R. F. 1984, *ApJ*, 277, 355
- Whelan, J., & Iben, I. J. 1973, *ApJ*, 186, 1007
- York, D. G., et al. 2000, *AJ*, 120, 1579